WEST-EAST HIGH SPEED FLOW FIELD CONFERENCE
19-22, November 2007
Moscow, Russia

GRID-FREE KINETIC UPWIND SOLVER ON CHIMERA CLOUD OF POINTS

K. Anandhanarayanan

CFD Division, DOCD, Defence Research and Development Laboratory, Hyderabad, India.
Email: kanand_cfd@yahoo.com

Key words: grid-free method, kinetic scheme, chimera cloud, high speed flows, store-separation.

Abstract. Grid-free Euler solver is applied to simulate flow past flight vehicle configurations for aerodynamic characterization. The grid-free solver requires just a cloud of points within the computational domain and therefore, it is highly efficient in handling multi-body configurations. In the present approach, the complex configuration is decomposed into geometrically simple components and cloud of points is generated around each component. Then, these clouds are overlapped to get a chimera cloud of points around the configuration. The geometries with relative movement, such as separation of store from aircraft, are also handled efficiently using this approach with a preprocessor to blank solid points and to generate connectivity (a set of neighbours around each point). Lower-Upper Symmetric Gauss Seidel (LU-SGS) is implemented in the grid-free solver and it is parallelized in Single Program Multiple Data (SPMD) environment using Message Passing Interface (MPI) to reduce the simulation time. The parallel grid-free Euler solver has been applied to study the control surface deflections characteristics of a flight vehicle, store-separation dynamics and nose panel separation of a hypersonic launch vehicle.

1. INTRODUCTION

Aerodynamic design of an aerospace vehicle using CFD codes involves a large number of numerical simulations of flow field around the vehicle at various flow conditions and geometric changes. The grid generation is a difficult and time consuming task for complex configurations. It becomes more difficult to generate grid for multi-body configurations. Further, the time required to generate grid is disproportionately very high in the simulation of time dependent study of relatively moving multi-body configurations. Chimera grid[1,2] approach has been proved to be very successful in such simulations, since the grid has to be generated once and component grids are overlapped at appropriate location during the dynamics. Even use of chimera grid also has some difficulty in tackling thin gaps between the overlapping geometries and interpolation of variables across the inter grid boundaries. Recently, the grid-free techniques have emerged as a new viable alternative to do computational analysis of various physical problems and provide greater flexibility to numerical analysis of many complex configurations. Least Squares Kinetic Upwind Method (LSKUM)[3,4] is popular among the grid-free methods to solve compressible flows. LSKUM does not require a grid for solving the governing partial differential equations; only points need to be distributed

over the domain. Higher order accuracy in space is achieved using the defect correction technique[5]. Dauhoo et. al. have extended the method to q-LSKUM[6] in which the entropy (q) variables are used in the defect correction step to get the second order accuracy in space. An Euler solver based on q-LSKUM has been developed and being applied to the design of flight vehicle configurations. Further, a continuous effort has been made to bring-out an efficient numerical simulation tool based on q-LSKUM to support in the flight vehicle design. The efforts include point distribution in the computational domain, implicit methods for faster convergence and parallelisation to reduce the turn-around time. The point distribution around the complex flight vehicles is obtained using overlapped grid approach in which the configuration is decomposed into geometrically simple components. Standard grid generation methods are used to generate the cloud of points around each component and the clouds are overlapped to get a distribution of points in the computational domain. Efficient blanking and search algorithms have been developed to generate the connectivity for each point. The convergence acceleration technique based on Lower-Upper Symmetric Gauss Seidel (LU-SGS) method has been modified in the LSKUM framework and implemented in the q-LSKUM code to get good speed-up without any extra memory[7]. Even though, the use of grid-free q-LSKUM reduces the grid generation time for a CFD analysis, the simulation of flow past a practical flight vehicle requires considerable CPU time for each flow condition. In order to reduce the time-to-solution, high performance CFD computations for large-scale realistic applications must be performed efficiently on state-of-the-art parallel supercomputers. The 3-D q-LSKUM code has been parallelized[8] on Single Program Multiple Data (SPMD) environment using Message Passing Interface (MPI). Parallel q-LSKUM code is being routinely applied to solve flow past multi-body flight vehicle configurations. This paper deals with generation of chimera cloud of points, connectivity generation and application to various multi-body configurations.

2. KINETIC FLUX VECTOR SPLITTING (KFVS)

Least Squares Kinetic Upwind Method (LSKUM)[3] is a kinetic scheme, which is based on the fact that the continuum gasdynamic equations are the moments of Boltzmann equation of kinetic theory of gases. Consider the Boltzmann equation,

$$\frac{\partial f}{\partial t} + \vec{v}\frac{\partial f}{\partial \vec{x}} = J \tag{1}$$

where f is the velocity distribution function, $\vec{v}(v^1, v^2, v^3)$ is the molecular velocity, $\vec{x}(x^1, x^2, x^3)$ is the spatial coordinate and J represents a collision term which vanishes in the thermodynamic equilibrium (Euler limit). The velocity distribution function f in this state becomes Maxwellian F and is given by

$$F = \frac{\rho}{I_o}\left(\frac{\beta}{\pi}\right)^{3/2} \exp\left[-\beta\left\|\vec{v} - \vec{u}\right\|^2 - \frac{I}{I_o}\right] \tag{2}$$

where $\beta = 1/(2RT)$, and I is the internal energy due to non-translational degrees of freedom, $I_o = (3-\gamma)/(2(\gamma-1))RT$ and $\vec{u}(u^1, u^2, u^3)$ is the fluid velocity. Here R is the gas constant, T is the fluid temperature and γ is the ratio of specific heats. In the Euler limit the Eq. (1) becomes

$$\frac{\partial F}{\partial t} + \vec{v}\frac{\partial F}{\partial \vec{x}} = 0 \tag{3}$$

By taking moments of Eq. (3), we get the Euler equations

$$\left\langle \Psi , \frac{\partial F}{\partial t} + \vec{v}\frac{\partial F}{\partial \vec{x}} \right\rangle = \frac{\partial U}{\partial t} + \frac{\partial \vec{G}}{\partial \vec{x}} = 0 \tag{4}$$

where U is the vector of conserved variables, $\vec{G}$ is the flux vector and they are given by

$$\begin{aligned} U &= \left[\rho, \rho\vec{u}, \rho e \right]^T \\ \vec{G} &= \left[\rho\vec{u}, \rho\vec{u}\otimes\vec{u} + p\bar{\bar{I}}, (\rho e + p)\vec{u} \right]^T \\ e &= \frac{RT}{(\gamma - 1)} + \frac{1}{2}\left\| \vec{u} \right\|^2 \\ p &= \rho RT \end{aligned} \tag{5}$$

Here ρ is the fluid density, p is the pressure and e is the internal energy.

The moment is defined as

$$\left\langle \Psi, F \right\rangle \equiv \int_0^\infty dI \int_{-\infty}^{\infty} d\vec{v}\, \Psi F \tag{6}$$

where the moment vector ψ is defined as

$$\Psi = \begin{bmatrix} 1, \vec{v}, I + \dfrac{\left\| \vec{v} \right\|^2}{2} \end{bmatrix}^T \tag{7}$$

The Kinetic Flux Vector Splitting (KFVS)[10] scheme can be constructed by splitting the Eq. (3) based on the sign of molecular velocity as

$$\frac{\partial F}{\partial t} + \frac{\vec{v} + \left| \vec{v} \right|}{2}\frac{\partial F}{\partial \vec{x}} + \frac{\vec{v} - \left| \vec{v} \right|}{2}\frac{\partial F}{\partial \vec{x}} = 0 \tag{8}$$

and taking ψ - moments of Eq. (8), the Euler equations can be obtained in split flux form as

$$\frac{\partial U}{\partial t} + \frac{\partial \vec{G}^{+}}{\partial \vec{x}} + \frac{\partial \vec{G}^{-}}{\partial \vec{x}} = 0 \tag{9}$$

where, $\vec{G}^{\pm}$ are the KFVS fluxes[10].

3. LEAST SQUARES KINETIC UPWIND METHOD (LSKUM)

The discretization of the spatial derivatives in Eq. (8) leads to various KFVS methods. In LSKUM[3], the spatial derivatives at a node P_o using weighted least squares in terms of data at neighbouring points, $P_i \in N(P_o)$. Using Taylor's expansion of F about P_o, we get

$$F_i = F_o + \Delta\vec{x}_i \cdot \vec{\nabla} F + O\left(\left|\Delta\vec{x}_i\right|^2\right), \qquad \Delta\vec{x}_i = \vec{x}_i - \vec{x}_o \tag{10}$$

The least squares approximation for $\vec{\nabla} F_i$ is obtained from the following weighted minimization:

$$\text{minimize} \sum_{i \in N(P_o)} w_i \left[F_i - F_o - \Delta\vec{x}_i \cdot \vec{\nabla} F_o \right]^2, \qquad \text{w.r.t.} \vec{\nabla} F_o \tag{11}$$

This gives a linear system of equations, $\mathbf{A}_o \vec{\nabla} F_o = b_o$, where $\mathbf{A}_o$ is a square matrix that depends only on the co-ordinates of node P_o and its neighbours. In the present work, the weight function is chosen as $w_i = \left\| \vec{x}_i - \vec{x}_o \right\|^{-2}$. The matrix $\mathbf{A}_o$ is symmetric and positive definite as long as the connectivity is non-degenerate; hence a unique solution exists. The solution to the above system of equations is obtained using Q-R factorization method. In LSKUM, the upwinding is introduced through the split stencil[4], i.e., the set of neighbours $N(P_o)$ is divided into subsets, such that $N_j^+ = \{P_i \in N(P_o),\ x_i^j \le x_o^j\}$ and $N_j^- = \{P_i \in N(P_o),\ x_i^j \ge x_o^j\}$ as shown in Fig. 1. The second term in Eq. (8) is evaluated using the points N_j^+ and the third term is evaluated with the points N_j^-. It is analogous to using the backward difference for the convective terms when the advection velocity is positive. After taking ψ - moments of the above discretised equation lead to the discretised approximation to the Euler equations.

The second order accuracy in space is obtained through the defect correction method[5]. It is a two step method and in the first step, the first order derivatives are obtained as mentioned above. Then we define

$$\begin{aligned} &\Delta\widetilde{F}_i = \widetilde{F}_i - \widetilde{F}_o, \qquad \textit{where} \\ &\widetilde{F}_i = F_i - \frac{\Delta\vec{x}_i}{2} \cdot \left. \frac{\partial F}{\partial \vec{x}} \right|_i \\ &\widetilde{F}_o = F_o - \frac{\Delta\vec{x}_i}{2} \cdot \left. \frac{\partial F}{\partial \vec{x}} \right|_o \end{aligned} \tag{12}$$

Using $\tilde{F}_o$ and $\tilde{F}_i$ instead of F_o and F_i in Eq. (11), second order accurate estimate for the derivatives of F can be obtained. It can be observed that the first order method uses non-negative Maxwellian distribution (F) which ensures the positivity of the fluid pressure and density[9]. The distribution functions ($\tilde{F}$) used in the defect correction step of LSKUM may not be a non-negative distribution function and also applying the defect correction to near wall points is difficult[11]. Therefore, the entropy variables, also known as q-variables, introduced by Deshpande[12] while studying the symmetric hyperbolic form of Euler equations are used in the defect correction step to get the second order accurate LSKUM known as q-LSKUM[6]. The q-variables are given by,

$$q=\begin{Bmatrix} \ln\rho+\dfrac{\ln\beta}{(\gamma-1)}-\beta\left\|\vec{u}\right\|^2 \\ 2\beta\vec{u} \\ -2\beta \end{Bmatrix} \tag{13}$$

In q-LSKUM, in the first step, derivatives of q-variables are obtained using least squares method with full stencil and the q-variables are modified using the defect correction method, similar to Eq. (12). The modified q-variables are used in constructing $\Delta\widetilde{F}=F(\widetilde{q}_i)-F(\widetilde{q}_o)$ to get the formal second order accurate estimates of derivatives of *F*. Thus the least squares formulae for first and second order LSKUM have the same structure, the only difference being use of modified Maxwellians. Therefore, the second order accurate q-LSKUM might inherit good properties of first order LSKUM such as robustness, smoothness of contours, positivity of density and pressure[11].

4. GENERATION OF DATA-STRUCTURE

Important tasks in handling multi-body configurations using the grid-free solver are distribution of points in the domain and generation of connectivity for each point. The distribution of points is obtained using chimera cloud method. In this method, the complex geometry is decomposed into geometrically simple components and 3-D structured / unstructured grids are generated around each component. These grids are overlapped to get the distribution of points within the domain. Due to overlapping of different component grids, some of the cells are cut by the surface of other components and such cut cells are identified. There are two types of cut cells present in the overlapped grids. In the first type, the cut cells are partially inside another component and partially outside, in such cases one or more vertices will be completely inside the component. All the vertices of cut cells are passed through the surface normal test[13]. The vertices inside the component are flagged as solid nodes and other vertices are flagged as fringe nodes. (The classification of fringe nodes has significance only to get neighbours from the overlapping grid. Once the connectivity is generated, the fringe nodes are also treated like any other interior or boundary nodes, whereas the governing equations are not solved at solid nodes.) In the second type of cut cells, the cut cell pierce through the geometry and all the nodes are interior nodes to the domain. Such cut cells are possible in the case of thin cutting surfaces and surfaces with discontinuities such as trailing edge of a wing or vertex of a cone. All the vertices of such cut cells are flagged as fringe nodes. The connectivity of such vertices will not include the vertices of the same cut cell that are in the opposite side of the cutting surface. The cells that are completely outside of other components are identified using painting algorithm and their vertices are flagged as active nodes. The nodes that are neither active nor fringe are flagged as solid nodes. In the overlapping grid one or more component grids, referred as minor grids, are completely submerged within a large grid referred as major grid. The nodes on the outer boundary of the minor grids also require connectivity from the overlapping grids. Therefore, such nodes are also flagged as fringe nodes. The connectivity to the active nodes can be obtained using the grid information and the solid nodes do not require any neighbour. The connectivity to fringe nodes includes neighbours in the same grid that are not flagged as solid node as well as in the same side

of the cutting surface and closest nodes from the overlapping grids. The closest nodes are obtained using octtree approach[14] or gradient search method[15,16].

5. CODE DEVELOPMENT AND APPLICATIONS

A 3-D grid-free Euler code has been developed using q-LSKUM. The code operates on a distribution of points. As mentioned earlier, q-LSKUM uses split stencils to evaluate the derivatives and therefore, the standard approximation to split flux Jacobians in LU-SGS method does not lead to diagonal matrices which would involve inversion of 5x5 matrixes at each point. Therefore, the split flux Jacobians are approximated to their spectral radii to get the simple diagonal matrices[7]. The modified LU-SGS has been implemented in q-LSKUM code to get faster convergence. Further, the code has been parallelized in SPMD computers using MPI libraries. The implicit, parallel grid-free code works for any complex geometry with same ease as solving simple geometries[8]. The implicit parallel q-LSKUM code is being routinely used in the design of flight vehicle configurations and some of the applications to multi-body configurations are presented here.

5.1. Hinge moment reduction of a flight vehicle

Prediction of hinge moment of the control surfaces of a flight vehicle is necessary for the selection of control actuator. Alternatively, the location of hinge line of the control surface will be decided to meet the available control actuator power. q-LSKUM Euler code has been used to predict the hinge moment of a flight vehicle configuration with deflected fins and a study has been carried out to reduce the hinge moment by shifting the control surface. The flight vehicle configuration consists of a blunt-ogive cylinder body with cruciform wings and all movable control surfaces (Fig. 2). Clouds of points are generated around the body, wings and fins (control surfaces) separately and overlapped to get a chimera cloud of points (Fig. 3). The fin clouds are moved to different fin positions and rotated about the hinge line to simulate the fin translation and deflection. The points that lie inside the solid body are removed using blanking algorithm. After blanking solid points, about 0.7 million points are available in the computational domain. The connectivity has been generated using gradient search algorithm.

The 3-D q-LSKUM code has been applied to simulate the flow past flight configuration at freestream Mach number $M_\infty = 1.2$, angle of attack $\alpha = 18^o$ and fin deflection angle $\delta = 0^o$, 6^o and 12^o and roll angle $\phi = 0^o$. The predicted maximum hinge moment at sea-level condition is 2.4 times the control actuator power at 12^o fin deflection angle. The reduction of hinge moment is possible by modifying the fin geometry or decreasing the distance between the center of pressure of the fin and the hinge line. The latter approach is followed in this study. The hinge line is fixed due to the space available for the control actuator. Therefore, the fin was moved forward to reduce the distance of center of pressure of fin from the hinge line. Numerical simulation has been carried out at two different fin locations such that the hinge moment is reduced to one-third of present hinge moment and the extreme case of nearly zero hinge moment. These cases correspond to forward movement of the fin about 0.08 and 0.11 times of diameter of the vehicle from the present location. The hinge moment at different fin positions is given in Fig. 4. As expected, the fin hinge moments have decreased to the expected values for the new positions of the fin. Further, the study has been carried out at Mach numbers

M_∞ = 0.8, 2.0 and 2.5. It is observed that the change in normal force and pitching moment are less than 1.7% and 2.5% respectively due to shift in the fin position[17]. Therefore, the effect of shift in fin position on the configuration performance parameters is only marginal. Effect of fin position on fin hinge moment is shown in Fig. 4 at different freestream Mach numbers. There is a considerable increase in hinge moment at higher Mach numbers due to high dynamic pressure. It is observed that the hinge moment drastically reduces due to the forward movement of the fin. It can be seen from the figure that the fin has to be moved forward about 0.13 diameters from the present fin position to meet the control power at all Mach number conditions.

5.2. Store separation dynamics

The q-LSKUM code has been integrated with 6-DOF trajectory equations of motion module to simulate the store separation dynamics. The integrated code has been validated for a generic store separating from a wing-pylon configuration (Fig. 5) at Mach 1.2. The experimental results[18] such as trajectory information and the surface pressure distributions are available for this test case. The configuration consists of a 45 degree clipped delta wing with NACA 64A010 airfoil section and an ogive-flat plate-ogive pylon. The store consists of a tangent-ogive fore-body, clipped tangent-ogive aft-body, and cylindrical section center-body. The store has cruciform fin of a 45 degree sweep clipped delta wing with NACA 008 airfoil section. Similar to the experimental set-up, a small gap exists between the store body and the pylon while in carriage. As in the experimental tests, a sting is attached to the store aft-body. Forward and aft ejectors are used to quickly accelerate the store away from the pylon. The store has an inherent nose down pitching moment. Therefore to counter this moment, the force exerted by the aft ejector force is more than the forward ejector.

Unstructured grids are generated around the wing-pylon and store with 26,516 and 16,148 points respectively. The grids are overlapped to get the chimera cloud of points as shown in Fig. 6. The study has been carried out with time step of 0.001 seconds till 0.3 seconds and the chimera cloud of points at various instants of time is shown in Fig. 7. The grid-free q-LSKUM Euler solver has been applied to obtain the flow-field. The surface pressure distributions at various instant of time are shown in Fig. 8 and the pressure distribution is integrated to get the aerodynamic forces and moments. The 6-DOF equations of motion are solved using the aerodynamic forces and moments to obtain the store trajectory. The linear displacement of the store is shown in Fig. 9 along with the experimental values. As expected, the vertical displacement is faster due to ejector force and the acceleration of gravity. Also, there is a small negative displacement due to the drag. The store angular rate is compared in Fig. 10. The initial pitch up moment due to ejector force can be observed and then due to inherent pitch down moment of the store, pitch angle decreases. The surface pressure distribution is also compared with the experimental result at two circumferential locations and at two time instants. The circumferential locations are denoted by the angle Φ. $\Phi = 0$ is located at the top ($y = 0$, nearer to the pylon) of the store while in carriage and is measured counter clockwise when viewed from the upstream. Figs. 11 and 12 show the pressure distributions at $\Phi = 5^o$ and 185^o, at t =0.0s and 0.16s. The surface pressure distribution is also compare well with the experimental values.

5.3. Nose panel separation dynamics

An airframe integrated scramjet engine (cruise vehicle) is carried to an altitude of 32.5km with the help of a launch vehicle and launched at Mach number 6.5 to

demonstrate the autonomous function of the scramjet combustor. The cruise vehicle is kept in the nose portion of the launch vehicle and the nose panels are separated before launching of the cruise vehicle as shown in Fig. 13. The nose panels are attached to the launch vehicle through a hinge at the end of the panels and are opened using a pyro mechanism to a small angle against the external aerodynamic forces. As the flow rushes through, the panels open up further due to the aerodynamic load. The panels should be detached at an optimum angle for safe separation from the launch vehicle. It is necessary to estimate the minimum opening angle required to initiate the opening and the maximum angle at which the panels can be separated safely without hitting the launch vehicle. It is very difficult and costlier to simulate such separation studies through experiments. Therefore, a CFD study has been carried out to estimate the aerodynamic loads and moments acting on the nose panels at different opening angles[19].

Unstructured grids are generated around the launch vehicle with cruise vehicle and two nose panels with size 981 thousand, 35 thousand and 21 thousand points respectively. The nose panel grid blocks are rotated about their respective hinge line to the desired angles and overlapped on the launch vehicle grid. The overlapped grids are shown in Figs. 14 and 15. The grid-free q-LSKUM code has been applied on the overlapped cloud to simulate the flow past full configuration. The simulation has been carried out at various included angles ranging from 1^o to 160^o. Figs. 16 and 17 show Mach contours and pressure contours in the yaw plane respectively for the opening angle 90^o. It can be observed that an attached oblique shock in front of panel 1 and a detached shock in front of panel 2 due to nose bluntness. These shocks interact with cruise vehicle shock and forms strong normal shock. A triple point shock structure near to panel 1 can be observed. Due to Mach reflection, a strong pressure rise on the panel can also be observed in the pressure contours, which in turn increases the aerodynamic load. The aerodynamic force and moment coefficients acting on the nose panels are estimated at various opening angles. The coefficient of force acting on the panels in the z-axis and the moment about hinge line are plotted in Figs. 18 and 19. Results indicate that both panels have a tendency to open even at 1^o and the maximum force occurs at 120^o to release the panels for safe separation. The moment increases monotonically with opening angles.

6. CONCLUSIONS

The 3-D grid-free Euler solver based on q-LSKUM code has been applied to multi-body configurations. The point distribution is obtained using chimera cloud method in which clouds of points are generated around geometrically simple components and overlapped. An efficient preprocessor has been used to generate the connectivity. The flows past multi-body configurations with relatively moving components are efficiently simulated using the grid-free solver. Three geometrically complex test cases have been solved using the grid-free solver and it is shown that the grid-free solver is an effective tool in handling multi-body configurations.

7. ACKNOWLEDGEMENTS

The author expresses his sincere gratitude to Director, DRDL, Technology Director, Computational Dynamics and Head, CFD Division for their support during the work. The author is grateful to G. Harish, M. Pavanakumar, R.R. More and S. Mondal for

their contributions in the development of preprocessor and simulation of store separation dynamics.

8. REFERENCES

[1] J. L. Steger and J.A. Benek, "On the use of composite grid schemes in computational aerodynamics", Comp. Meth. in App. Mech. and Engg., 64, 301-320, (1987).

[2] Z.J. Wang, and V. Parthasarathy, A fully automated chimera methodology for multiple moving body problems, Int. Jnl. for Num. Meth. in Fluids, 33, 919-938, (2000).

[3] S.M. Deshpande, A.K. Ghosh and J.C. Mandal, "Least square weak upwind methods for Euler equations", Report No. 89 FM4, Department of Aerospace Engineering, IISc, Bangalore, (1989).

[4] A.K. Ghosh and S.M. Deshpande, "Least squares kinetic upwind method for inviscid compressible flows" AIAA Paper No. 95-1735, (1995).

[5] S.M. Deshpande, "Meshless method, accuracy, symmetry breaking, upwinding and LSKUM", FM report no. 2003 FM 1, Dept. of Aerospace Engg., Indian Institute of Science, Bangalore, (2003).

[6] M.Z. Dauhoo, A.K. Ghosh, V. Ramesh and S.M. Deshpande, "q-LSKUM - A new higher order kinetic upwind method for Euler equations using entropy variables", Computational Fluid Dynamics Journal, 9, (2000).

[7] K. Anandhanarayanan, M. Nagarathinam and S.M. Deshpande, "An Entropy Variable-Based Grid-free Euler Solver with LU-SGS Accelerator", Proceedings of 24th ICAS Congress, Yokohama, Japan , (2004).

[8] K. Anandhanarayanan, M. Nagarathinam and S.M. Deshpande, "Parallelisation of a Grid-free Kinetic Upwind Solver", AIAA paper No. 2005-4846, (2005).

[9] S.M. Deshpande, "Kinetic theory based new upwind methods for inviscid compressible flows", AIAA Paper No. 86-0275, (1986).

[10] J.C. Mandal, and S.M. Deshpande, "Kinetic flux vector splitting for Euler equations", Computers & Fluids Journal, 23, 447-478 (1994).

[11] S.M. Deshpande, K. Anandhanarayanan, C. Praveen and V. Ramesh, "Theory and Applications of 3-D LSKUM Based on Entropy Variables", Int. Jnl. of Numerical Methods in Fluids, 40, 47-62 (2002).

[12] S.M. Deshpande, "On the Maxwellian distribution, symmetric form and entropy conservation for the Euler equations", NASA Technical Paper 2583, NASA, (1986).

[13] R.L. Meakin,"Composite overset structured grids", Handbook of grid generation, edited by J.F. Thompson, N.P. Weatherill, and B. Soni, pp. 11.1 - 11.20, (1999).

[14] G. Harish, M. Pavanakumar, and K. Anandhanarayanan, "Store separation dynamics using grid-free Euler solver", AIAA Paper No. 2006-3650, (2006).

[15] K. Anandhanarayanan, M. Nagarathinam, S.M. Deshpande, "Development and applications of a grid-free kinetic upwind solver to multi-body configurations", AIAA paper No. AIAA 2005-4628, (2005).

[16] R.R. More, and K. Anandhanarayanan, "Development of a preprocessor to generate data structure using overlapped grids", DRDL Report No. DRDL/5261/DOCD/CFD/TECH/07-03, (2007).

[17] K. Anandhanarayanan, "Fin Hinge Moment Reductions of a Flight Vehicle Configuration using Grid-Free Euler Solver", 9th Annual CFD Symposium of Aeronautical Society of India, Bangalore, India, Aug 2006.

[18] R.R. Heim, "CFD wing/ pylon/ finned store mutual interference wind tunnel experiment,"AEDC-TSR-91-P4, (1991).

[19] R.R. More, S. Srinivasa Raju, K. Anandhanarayanan and R. Krishnamurthy, "Nose panel opening study of a hypersonic vehicle", Proceeding of International conference on high speed high speed transatmospheric air & space transportation, Hyderabad, India, 29-30, June (2007)

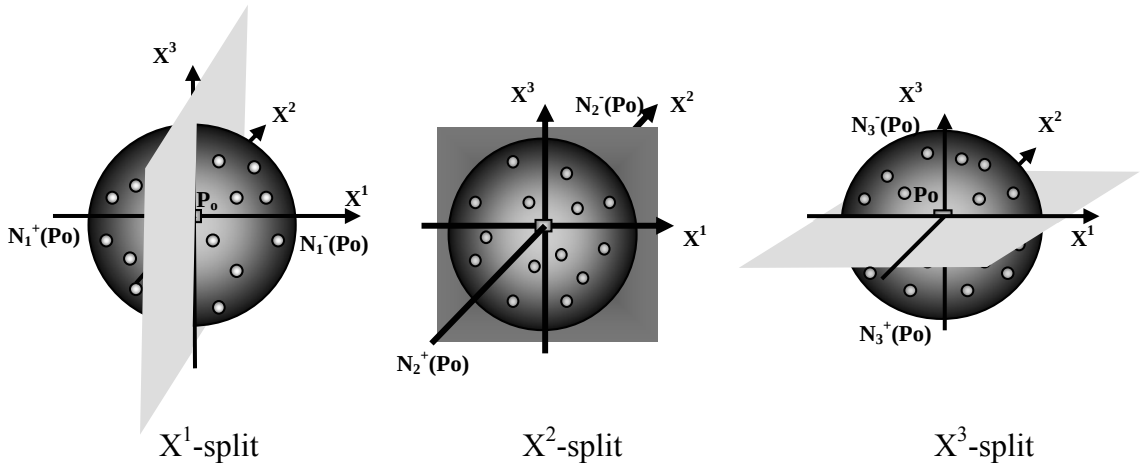

Figure 1. Split stencil definition

Figure 2. Geometry of flight vehicle configuration

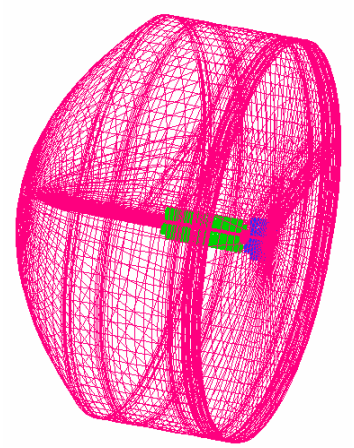

Figure 3. Overlapped cloud of points

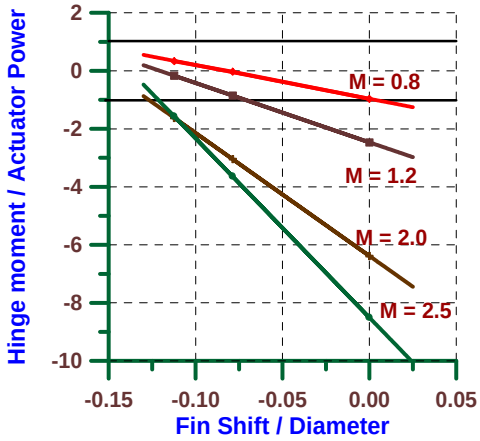

Figure 4. Fin hinge moment with fin position

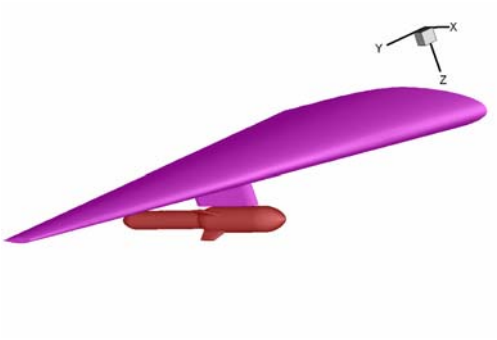

Figure 5. Wing-pylon store geometry

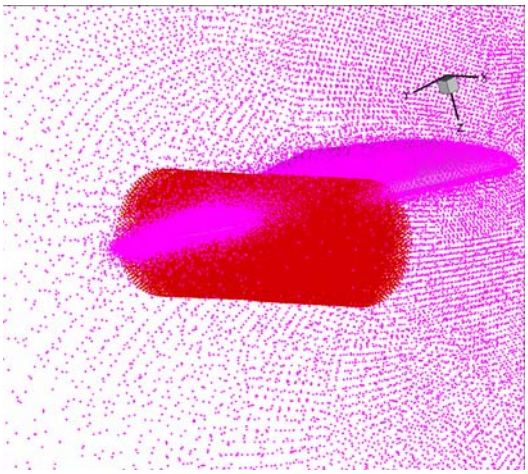

Figure 6. Initial chimera cloud of points

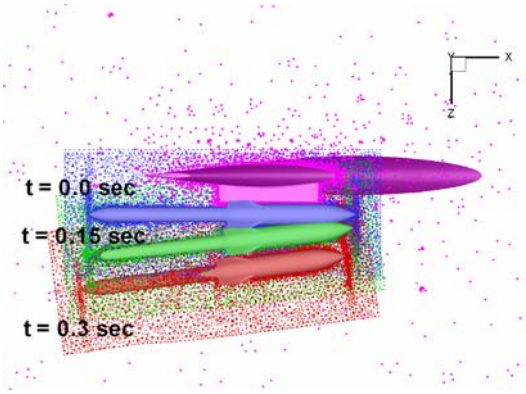

Figure 7. Chimera clouds at various instant of time

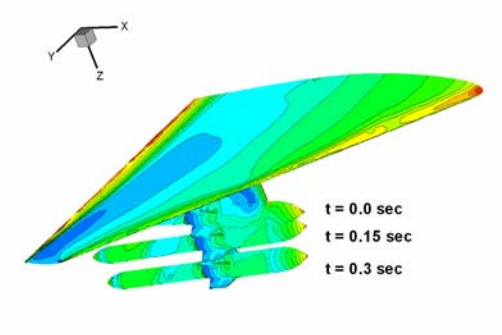

Figure 8. Surface pressure distribution

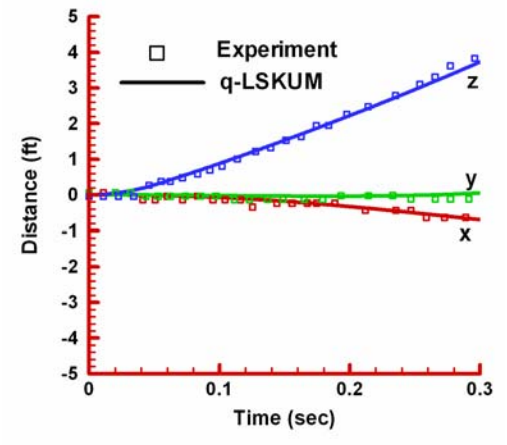

Figure 9. Linear displacement of store with time

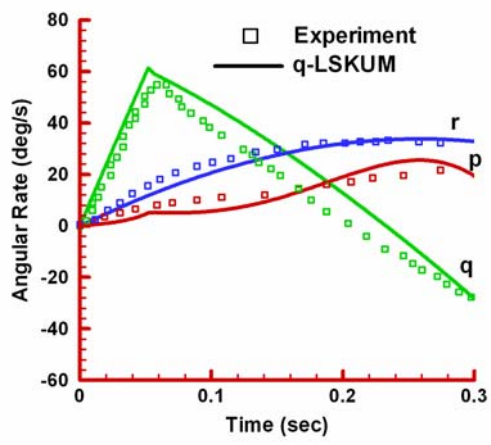

Figure 10. Angular rates of store with time

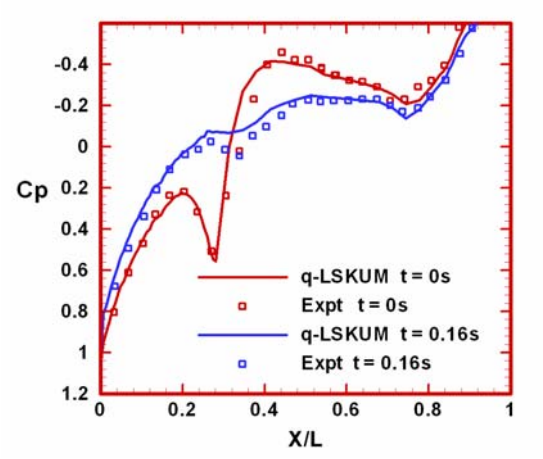

Figure 11. Surface pressure distribution at $\Phi = 5^{o}$

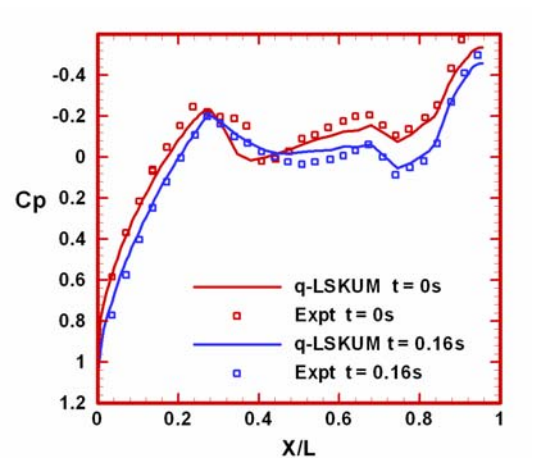

Figure 12. Surface pressure distribution at $\Phi = 185^{o}$

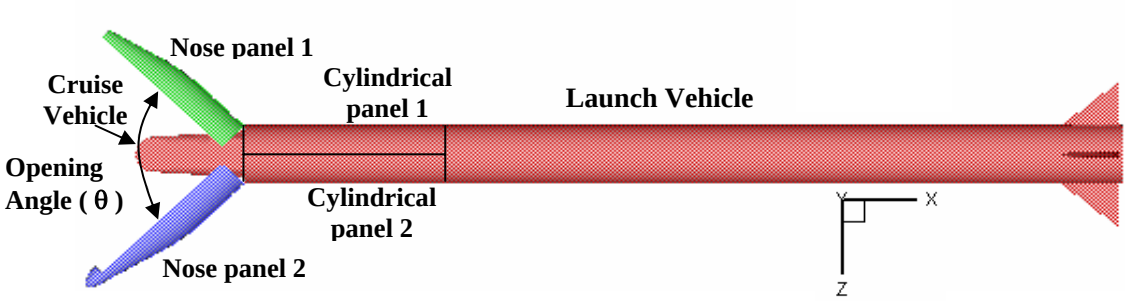

Figure 13. Launch vehicle with cruise vehicle and nose panels

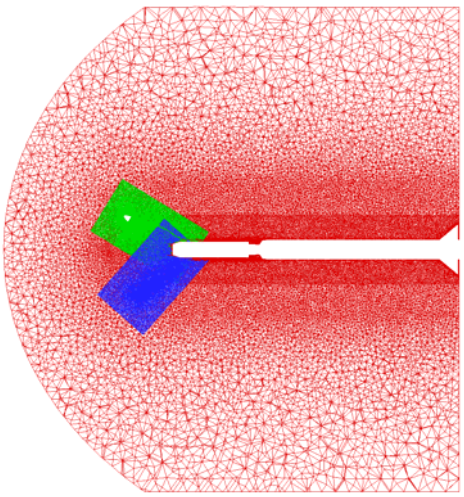

Figure 14. Overlapped unstructured grids

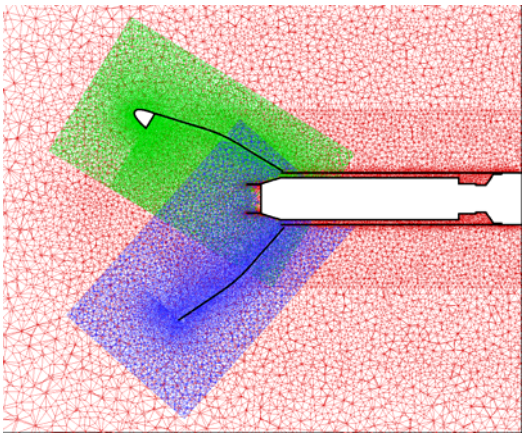

Figure 15. Zoomed view of overlapped grids

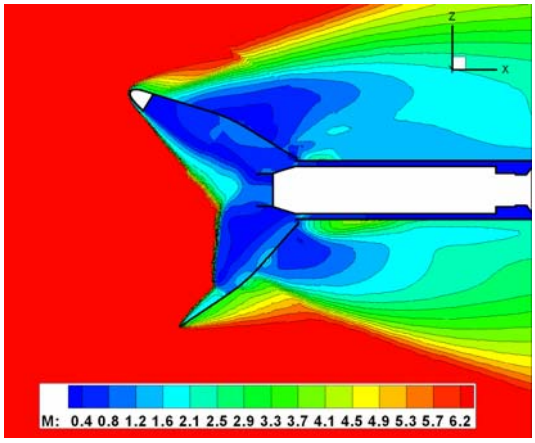

Figure 16. Mach contours in yaw plane

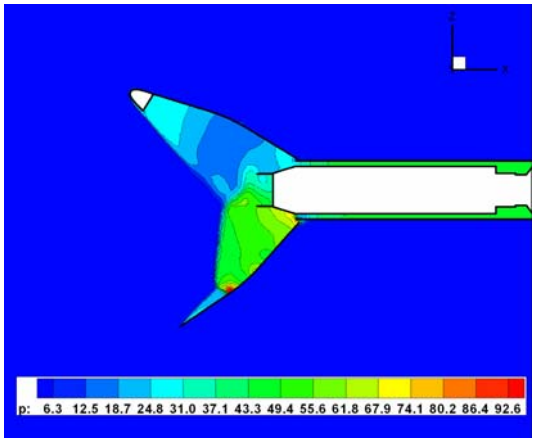

Figure 17. Pressure contours in yaw plane

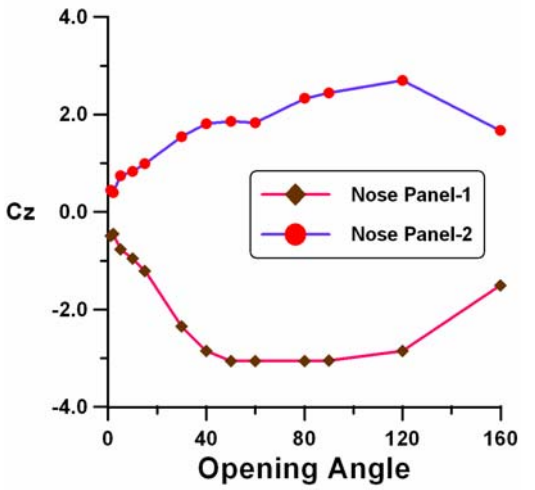

Figure 18. Coefficient of force along the z-axis

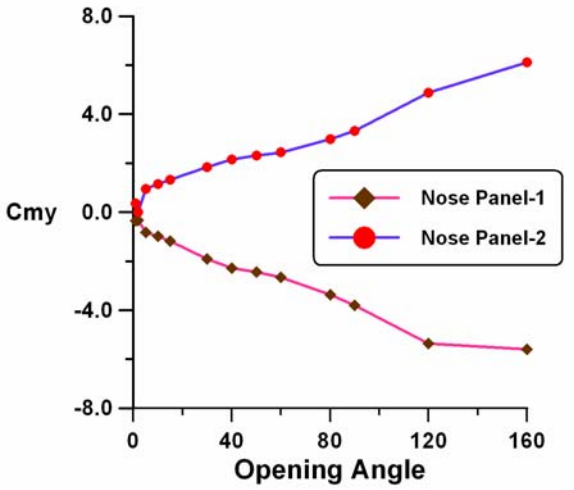

Figure 19. Coefficient of moment about hinge line